Viscoelasticity and Stokes-Einstein relation in repulsive and attractive colloidal glasses

Antonio M. Puertas,[1] Cristiano De Michele,[2] Francesco Sciortino,[2] Piero Tartaglia,[3] and Emanuela Zaccarelli[2]

[1]*Group of Complex Fluids Physics, Departamento de Física Aplicada,*
Universidad de Almería, 04120 Almería, Andalucía, SPAIN
[2]*Dipartimento di Fisica, Istituto Nazionale per la Fisica della Materia, and CNR-INFM-SOFT,*
Università di Roma La Sapienza, Piazzale Aldo Moro 2, I-00185, Roma, Italy
[3]*Dipartimento di Fisica, Istituto Nazionale per la Fisica della Materia, and CNR-INFM-SMC,*
Università di Roma La Sapienza, Piazzale Aldo Moro 2, I-00185, Roma, Italy
(Dated: February 5, 2008)

We report a numerical investigation of the visco-elastic behavior in models for steric repulsive and short-range attractive colloidal suspensions, along different paths in the attraction-strength vs packing fraction plane. More specifically, we study the behavior of the viscosity (and its frequency dependence) on approaching the repulsive glass, the attractive glass and in the re-entrant region where viscosity shows a non monotonic behavior on increasing attraction strength. On approaching the glass lines, the increase of the viscosity is consistent with a power-law divergence with the same exponent and critical packing fraction previously obtained for the divergence of the density fluctuations. Based on mode-coupling calculations, we associate the increase of the viscosity with specific contributions from different length scales. We also show that the results are independent on the microscopic dynamics by comparing newtonian and brownian simulations for the same model. Finally we evaluate the Stokes-Einstein relation approaching both glass transitions, finding a clear breakdown which is particularly strong for the case of the attractive glass.

I. INTRODUCTION

Understanding dynamic arrest in colloidal system is crucial in disparate technological applications (e.g. food industry[1], biomaterials[2], painting). Development of basic science also requires a deeper understanding of the different routes and mechanisms leading to dynamic arrest (glasses and gels)[3, 4, 5, 6]. In this respect, model colloidal systems are playing a very important role due to their versatility. It is indeed possible to tailor the shape, size and structure of the colloidal particles making it possible to design specific colloidal interaction potentials[7]. Furthermore, accurate experimental methods are now available for investigating the structure and the dynamics of colloids even at the single particle level[8]. Unexpected novel behaviors regarding the glass transition have been theoretically predicted[9, 10, 11, 12, 13] and experimentally observed[14, 15, 16, 17, 18, 19] in the cases in which colloidal particles interact, beside the hard-core, via a short-range attractive interaction potentials (when the attraction range is about one tenth of the particle diameter or less). The predictions, based on application of the mode coupling theory for supercooled liquids (MCT)[20] suggest that the standard packing-driven hard-sphere glass transition transforms – discontinuously in some cases – into a novel-type of glass transition driven by the short-range attraction. The competition between the two different arrest mechanisms introduces slow-dynamics features which are not commonly observed in molecular and atomic systems. Experiments on solutions of (hard-sphere like) colloidal particles (either PMMA or polystyrene micronetwork spheres) in the presence of small non-adsorbing polymers [14, 15, 17] have shown that there exists a window of polymer densities in which the mobility of the colloidal particles has a maximum for a finite value of polymer concentration. Moreover, for small and large polymer concentrations, the strength of the α-relaxation (the non-ergodicity parameter) is found to be very different, suggesting that indeed the visco-elastic response of the repulsive and attractive glass will also be significantly different. Molecular dynamics simulations of short-ranged models[21, 22, 23, 24] have confirmed the picture resulting from the theoretical predictions and validated by the experiments. A recent review can help summarizing the experimental and numerical studies in short-range attractive colloids[5].

The numerical results have been so far mostly limited to the study of self and collective properties of the density fluctuations. Despite the strong link with experiments and the relevance to industrial applications, the numerical evaluation of the viscosity, η, and viscoelastic properties $\tilde{\eta}(\omega)$ have lagged behind, since significant computational effort is requested for accurate calculation of $\tilde{\eta}(\omega)$, even more for states close to dynamical arrest. Experimentally, measurements of η close to the repulsive hard-sphere glass transition show an apparent divergence, but there is no consensus on the functional form describing such increase[25, 26]. For colloidal gels, a power law divergence has been reported in connection to the gel transition [27]. Theoretically, MCT predicts an asymptotic power law divergence, with identical exponent, of all dynamical quantities with the distance from the transition, and hence η, the time scale of the density fluctuations τ and the inverse of the self diffusion coefficient $1/D_0$ should diverge with the same critical parameters.

In this article, we attempt a characterization of the viscoelastic properties of two different short-range attractive potentials (a polydisperse Asakura-Osawa and a square-well) along three different paths in the attraction strength-packing fraction plane, which allow us to

access both the repulsion driven and attraction driven glass transitions with both systems. We show the divergence of the viscosity, as well as the diffusion coefficient or structural relaxation time, as the repulsive and attractive glasses are approached. At high density, the isochoric path shows the reentrant glass; the viscosity increases about three orders of magnitude upon either increasing or decreasing the strength of attraction.

The article is organized as follow: in Sec. II we introduce the numerical models and describe the methods to calculate the viscosity. In Sec. III we describe the paths investigated and provide some background information on the behavior of the diffusion and collective density fluctuations along these paths. In Sec. IV we discuss the observed behavior of the viscosity on approaching the repulsive and the attractive glass lines. In Sec. V, guided by theoretical MCT predictions for the viscosity, we provide evidence that the visco-elastic behavior close to the two different glass lines is controlled by density fluctuation of different wavelength. Finally in Sec. VI we report a study of the density and attraction strength dependence of the Stoke-Einstein relation.

II. NUMERICAL SIMULATIONS

A. Model A: Square well and Hard Sphere Binary Mixture

We perform Molecular Dynamics (MD) simulations of a 50:50 binary mixture of 700 particles of mass m with diameters $\sigma_{AA} = 1.2$ and $\sigma_{BB} = 1$ (setting the unit of length). The particles interact through a hard core repulsion complemented by a narrow square well (SW) pair potential. The hard core repulsion for the AB interaction occurs at a distance $\sigma_{AB} = (\sigma_{AA} + \sigma_{BB})/2$. The SW potential is,

$$V_{SW}(r) = \begin{cases} \infty & r < \sigma_{ij} \\ -u_0 & \sigma_{ij} < r < \sigma_{ij} + \Delta_{ij} \\ 0 & r > \sigma_{ij} + \Delta_{ij} \end{cases} \quad (1)$$

where r is the distance between particles of types $i, j = A, B$, the depth of the well u_0 is set to 1 and the widths Δ_{ij} are such that $\Delta_{ij}/(\sigma_{ij} + \Delta_{ij}) = 0.03$. Temperature T is measured in units of u_0 ($k_B = 1$), the attraction strength $\Gamma = 1/T$, time t in $\sigma_{BB}(m/u_0)^{1/2}$. The use of a binary mixture allows us to suppress crystallization at high packing fraction $\phi = (\rho_A \sigma_A^3 + \rho_B \sigma_B^3) \cdot \pi/6$, where $\rho_i = N_i/L^3$, L being the box size and N_i the number of particles for each species. The system undergoes phase separation into a gas and a liquid for large attraction strength in a wide range of packing fractions [28]: the critical point is located roughly at $\Gamma_c \approx 3.33$ and $\phi_c \approx 0.27$ (the latter is estimated from the Noro-Frenkel scaling[29] invariance close to the Baxter limit[30]). Previous studies[23, 28, 31] of the same model allowed us to locate the dynamical arrest line and the spinodal curve.

The 'numerical' glass line was determined by extrapolation via a power-law fitting of the normalized diffusion coefficient D/D_0, i.e. $D/D_0 \sim (\phi - \phi_g)^\gamma$ [31], where $D_0 = \Gamma^{1/2}$. This study was complemented by the calculation of the MCT glass lines for the same model. Hence, a bilinear transformation of ϕ and T was used to to superimpose the theoretical onto the numerical glass line.

We also study, as discussed below, the same 50:50 binary mixture of 700 particles, with the same $\sigma_{AA}, \sigma_{BB}, \sigma_{AB}$ above, but interacting simply as hard spheres, for which the potential reads,

$$V_{HS}(r) = \begin{cases} \infty & r < \sigma_{ij} \\ 0 & r > \sigma_{ij}. \end{cases} \quad (2)$$

For Newtonian dynamics (ND) simulations, we used a standard event-driven (ED) algorithm[32]. We also perform Brownian Dynamics (BD) simulations of the same model, to ensure the independence of the viscoelastic calculations on the microscopic dynamics. For BD simulations we exploit a recently developed [33] BD algorithm, which we shortly describe below. For a more extensive discussion we invite the reader to consult Ref. [34].

If the position Langevin equation is considered, i.e.:

$$\dot{\mathbf{r}}_i(t) = \frac{D_0}{k_B T} \mathbf{f}_i(t) + \overset{\circ}{\mathbf{r}}_i(t), \quad (3)$$

where $\mathbf{r}_i(t)$ is the position of particle i, D_0 is the short-time (bare) diffusion coefficient, $\mathbf{f}_i(t)$ is the total force acting on the particle, $\overset{\circ}{\mathbf{r}}_i(t)$ a random thermal noise satisfying $< \overset{\circ}{\mathbf{r}}_i(t) \cdot \overset{\circ}{\mathbf{r}}_i(0) >= 6 D_0 \delta(t)$. The BD integration scheme of Eq. 3 can be schematized as follow:

(i) every $t_n = n\Delta t$ (n integer) extract velocities $\vec{v}_i$ according to a Maxwellian distribution of variance $\sqrt{k_B T/m}$;

(ii) evolve the system between t_n and $t_n + \Delta t$ according to the laws of ballistic motion (performing standard ED molecular dynamics).

In other words, Gaussian particle displacements $\Delta \vec{r}_i = \vec{v}_i \Delta t$ are extracted according to $\langle \Delta \vec{r}_i^2 \rangle = 6 D_0 \Delta t$ and between two velocities extractions, standard ED dynamics is applied.

The present binary mixture model allows us to study the viscoelastic properties within the reentrant liquid region, enclosed by the nearby attractive and repulsive glass transitions. On the other hand, due to phase separation, it does not allow us to approach the attractive glass line at moderate density. Hence we will study V_{HS} for varying ϕ (Path 1A in Fig. 1) and V_{SW} at fixed $\phi = 0.58$ on varying T (Path 3 in Fig. 1).

B. Model B: Asakura-Oosawa Polydisperse System

We also study an interaction potential based on the Asakura-Oosawa model to make a direct link with experiments in colloid-polymer mixtures. A polydisperse

system, comprised of 1000 particles, is simulated with the standard velocity Verlet algorithm for Newtonian Dynamics in the canonical ensemble, which requires a continuous differentiable potential. To this end, a soft core was used instead of the hard core in Model A:

$$V_{sc}(r) = (\sigma_{ij}/r)^{36} \quad (4)$$

where $\sigma_{ij} = (\sigma_i + \sigma_j)/2$, with σ_i the diameter of particle i. Diameters where distributed according to the flat distribution $[\sigma - \delta, \sigma + \delta]$ with σ the mean diameter and $\delta = 0.1\sigma$. The short-range attraction between particles is given by the Asakura-Oosawa model for polydisperse systems:

$$V_{AO}(r) = -k_B T \phi_p \left\{ \left[(\bar{\eta} + 1)^3 - \frac{3r}{2\xi}(\bar{\eta} + 1)^2 + \frac{r^3}{2\xi^3} \right] + \right.$$

$$\left. + \frac{3\xi}{8r}(\eta_1 - \eta_2)^2 \left[(\bar{\eta} + 1) - \frac{r}{\xi} \right]^2 \right\} \quad (5)$$

for $\sigma_{12} \leq r \leq \sigma_{12} + \xi$ and 0 for larger distances; $\eta_i = \sigma_i/\xi$, $\bar{\eta} = (\eta_1 + \eta_2)/2$, and ϕ_p is the volume fraction of the polymer. The range of the interaction, ξ, is the polymer size, and its strength is proportional to ϕ_p, the concentration of ideal polymers. To ensure that the interaction potential $V_{sc} + V_{AO}$ has its minimum at σ_{12}, the Asakura-Oosawa potential is connected analytically to a parabola at $\sigma_{12} + \xi/10$ [35]. For average particles, $\sigma_1 = \sigma_2 = \sigma$, the attraction strength of the Asakura-Oosawa potential is given by $V_{min} = -k_B T \phi_p (3/2\eta + 1)$, which for $\xi = 0.1$, is $V_{min} = -16 k_B T \phi_p$.

Because the attractive glass transition occurs inside the liquid-gas spinodal, it cannot be accessed directly from the fluid with this potential. Thus, we have added a long range repulsive barrier to the interaction potential that destabilizes a macroscopic separation into two fluid phases. The barrier is given by:

$$V_{bar}(r) = k_B T \left\{ \left(\frac{r - r_1}{r_0 - r_1} \right)^4 - 2 \left(\frac{r - r_1}{r_0 - r_1} \right)^2 + 1 \right\} \quad (6)$$

for $r_0 \leq r \leq r_2$ and zero otherwise, with $r_1 = (r_2 + r_0)/2$. The limits of the barrier were set to $r_0 = \sigma_{12} + \xi$, and $r_2 = 2\sigma$, and its height is $1 k_B T$. The barrier raises the energy of a dense phase, so that liquid-gas separation is suppressed. The resulting total interaction,

$$V_{tot}(r) = V_{sc}(t) + V_{AO}(r) + V_{bar}(r) \quad (7)$$

is analytical everywhere and allows straightforward integration of the equations of motion.

This model allows us to study the viscoelastic properties of the fluid close to the attraction driven glass transition at moderate density, i.e. far from the high order

singularity. We will use this system to approach the repulsive glass with increasing ϕ_c at $\phi_p = 0$, hence using simply V_{sc} (Path 1B in Fig. 1), as well as to study the attractive glass at moderate density $\phi_c = 0.40$ (Path 2 in Fig. 1) by using V_{tot}.

C. Computation of viscosity

The shear viscosity η is given by the Green-Kubo relation:

$$\eta \equiv \int_0^\infty dt\, C_{\sigma\sigma}(t) = \frac{\beta}{3V} \int_0^\infty dt \sum_{\alpha < \beta} \langle \sigma^{\alpha\beta}(t)\sigma^{\alpha\beta}(0) \rangle, \quad (8)$$

which expresses η as the integral of the correlation function of the non-diagonal terms of the microscopic stress tensor, $\sigma^{\alpha\beta} = \sum_{i=1}^N m v_{i\alpha} v_{i\beta} - \sum_{i<j}^N \frac{r_{ij\alpha} r_{ij\beta}}{r_{ij}} V'(r_{ij})$, where V is the volume of the simulation box, $v_{i\alpha}$ is the α-th component of the velocity of particle i, and V' is the derivative of the total potential. $\langle ... \rangle$ indicates an average over initial conditions. However, from the computational point of view it is more convenient to use the Einstein relation,

$$\eta = \lim_{t\to\infty} \eta(t) = \frac{\beta}{6V} \lim_{t\to\infty} \frac{1}{t} \langle \Delta A(t)^2 \rangle, \quad (9)$$

where $\Delta A(t)$ is the integral from 0 to t of the three off-diagonal terms of the stress tensor,

$$\Delta A(t) = A(s+t) - A(s) = \int_s^{s+t} \sum_{\alpha<\beta} \sigma^{\alpha\beta}(s')ds' \quad (10)$$

Using Eq.9 is analogous to the calculation of the diffusion coefficient as the long time slope of the mean squared displacement.

For discontinuous potentials (hard cores or square wells), equation 9 can still be used[36] despite the impulsive character of the interactions. In this case,

$$[\Delta A(t)]_{HS,SW} = \sum_{collisions} \sum_{\alpha\neq\beta} [(m\sum_{i=1}^N v_{i\alpha}v_{i\beta})\tau_t +$$

$$m(x_{k\alpha} - x_{l\alpha})(v_{k\beta}^{after} - v_{l\beta}^{before})] \quad (11)$$

where τ_t is the time elapsed from the previous collision, k and l are the two colliding particles, $x_{k\alpha}$ is the position of particle k in direction α, and $(v_{k\beta}^{after} - v_{l\beta}^{before})$ is the momentum change in direction β of particle k due to the collision with particle l. We have not attempted to numerically recover $C_{\sigma\sigma}(t)$ from $\Delta A(t)$.

D. Units

For both studied models we report states in the packing fraction vs. attraction strength plane ($\phi_c - \Gamma$). For

	ϕ_c^G	b	γ_τ	γ_D
Model A: V_{HS}	0.584	0.51	2.75	2.17
Model B: V_{sc}	0.594	0.53	2.72	2.02

TABLE I: Glass transition point ϕ_c^G, von Schweidler exponent b, and divergence exponents of the characteristic time of the decay of density fluctuations γ_τ and of the diffusion coefficient γ_D for models A and B in the absence of attraction, i.e. respectively V_{HS} and V_{sc}, along path 1.

	Γ^G	b	γ_τ	γ_D
Path 2: V_{tot}	9.099	0.37	3.23	1.23
Path 3: V_{SW}	3.56	0.33	3.75	2.2

TABLE II: Glass transition point Γ^G, von Schweidler exponent b, and divergence exponents γ_τ and γ_D for models A and B in the presence of attraction, i.e. V_{SW} and V_{tot}, along respectively path 3 and 2.

Model A, the attraction strength is given by the inverse temperature (for HS temperature is irrelevant and is set equal to 1), whereas for Model B, $\Gamma = -V_{min}$. Distances are measured using σ_{BB} for model A and the mean diameter, σ for model B, while the particle mass, m, is always set to one. The stress correlation function is measured in units of $k_B T/\sigma^3$, and time in units of $(\sigma^2 m/k_B T)^{1/2}$. The viscosity is thus given in $(mk_B T)^{1/2}/\sigma^2$. For the integration of the equations of motion in model B, the time step was set to $\delta t = 0.0025/\sqrt{3}$.

III. DESCRIPTION OF PATHS, TRANSITION, FITS, EXPONENTS

Using the models presented above, we numerically study the following paths schematized in Fig. 1:

Path 1: The zero-attraction case for both models, i.e. the hard- and the soft sphere models. The two models are not identical along this path because (i) the Asakura-Oosawa model has a soft repulsion (although the r^{-36}-core is quite hard and no important effects are expected [37]) and more importantly *ii*) the size distributions are different: bimodal in model A vs. continuous in model B. Model B has been studied previously along this path monitoring the self-diffusion and the density correlation functions[38]. The glass transition points and the exponents controlling the power-law divergence of the structural relaxation time scale, γ_τ, and the diffusion coefficient, γ_D, as well as the von Schweidler exponent b (which provides a measure of the slow-decay of the density correlation function), are shown in Table I for both systems. The difference in the critical packing fractions can be attributed to the different size distributions of the two models. The exponents γ_τ and γ_D, on the other hand, are very similar in both models.

Path 2: Approaching the attractive glass. This path is studied with model B, for which the liquid-gas transition is destabilized and the glass transition can be approached from the fluid. This path has been studied previously monitoring the density correlation functions [35, 39] and the viscosity [40], and the glass transition is found for $\Gamma^G = 9.099$; the associated von Schweidler and critical exponents are given in Table II.

Path 3: The reentrant region and the approach to the attractive glass. This path is studied with model A, at $\phi_c = 0.58$, a value well within the reentrant region[23]. The corresponding parameters for this path are provided

in Table II. At large temperature, the glass transition is approached but not reached because the studied packing fraction is close, but smaller than ϕ_c^G for V_{HS}, i.e. the path is parallel to the repulsive glass line in the limit $T \to \infty$.

Note that, as predicted from MCT, the attractive glass shows lower von Schweidler exponents than the repulsive glass, for both paths and models, while γ_τ is larger. This implies that the divergence of the time scale for structural relaxation is more abrupt. For the square well mixture, quantitative results from simulations and MCT are available[31], predicting the transition point at $\phi = 0.58$ for $\Gamma^{G,MCT} \simeq 3.70$, in quite good agreement with that estimated from the fits $\Gamma^G \simeq 3.56$. For path 2 a quantitative comparison with MCT has been also recently performed [41], showing that the driving mechanism for the slowing down observed in the simulation is driven by the short-range attractions (large-q modes of $S(q)$).
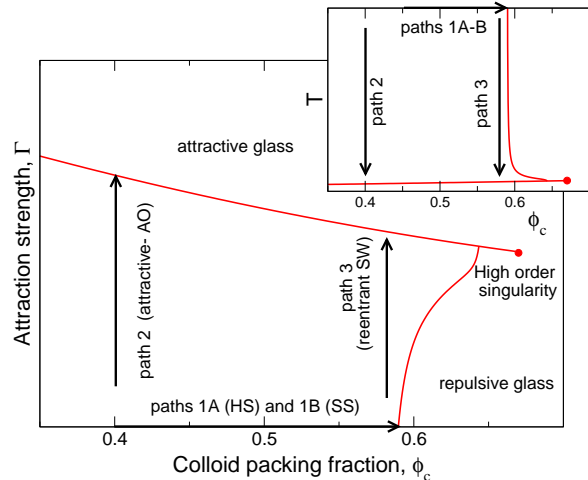

FIG. 1: Schematic phase diagram showing the attraction and repulsion driven glasses and the three paths followed in this work. Note that path 1 (infinite temperature limit) is studied within both models. The inset shows the three paths in the temperature-packing fraction representation.

IV. VISCOSITY RESULTS

In this section we study the viscosity along the three paths described above.

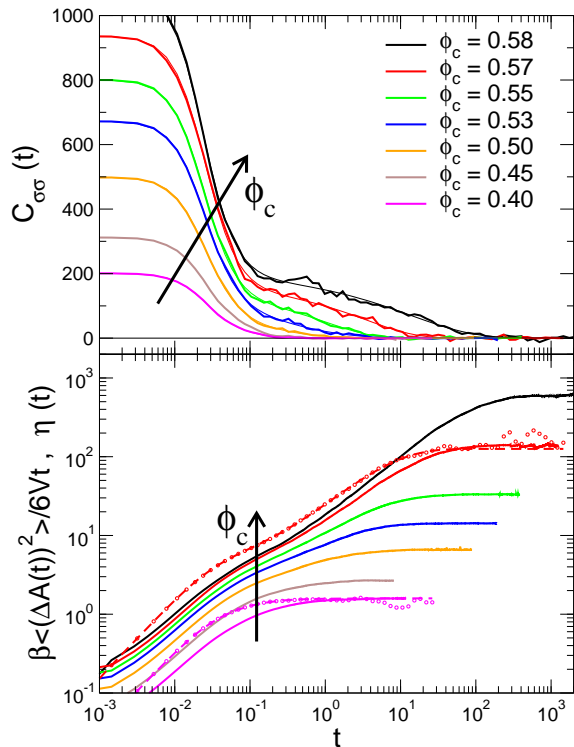## A. Hard and soft spheres: Paths 1A and 1B

FIG. 2: Upper panel: Stress correlation function $C_{\sigma\sigma}(t)$ for V_{sc}. The thin lines are empirical fittings to describe the data (see section V for details). Lower panel: Full lines are $\beta < (\Delta A(t))^2 > /6Vt$ (from the Einstein relation Eq. 9) for all studied ϕ_c. For two specific values of ϕ_c ($\phi_c = 0.57$ and $\phi_c = 0.40$) we also show $\eta(t)$ obtained using a direct integration of $C_{\sigma\sigma}(t)$ (symbols), and integration of the fitting curves (dashed thick). Note that while $\eta(t)$ and $\beta(\Delta A(t))^2/6Vt$ have the same long-time value, their time dependence is different.

In Figure 2 we present, along path $1B$, the stress correlation function for V_{sc} at different concentrations (upper panel), and the integral of the squared non-diagonal terms of the stress tensor (lower panel). The correlation functions have been averaged over 5000 independent calculations. Note the progressive development of a two-step decay in $C_{\sigma\sigma}(t)$ as the concentration increases and the glass transition is approached, with the second (structural) decay of $C_{\sigma\sigma}(t)$ moving to longer and longer times. This implies that stress relaxes slower and slower, or equivalently that the system increases its ability to store the stress; i.e. the system becomes viscoelastic. Additionally, it can be observed that $C_{\sigma\sigma}(0)$ grows close to the transition. Both effects are responsible for the increase of the viscosity upon increasing the packing fraction, but the increase in the time scale is the one providing the

leading contribution to the integral (see Eq. 8).

The integral of the stress correlation function is very noisy, and the numerical evaluation of the viscosity is more accurate if calculated using the Einstein relation (Eq. 9), as shown in the lower panel of Fig. 2. For comparison, the integral of the functional form used to describe $C_{\sigma\sigma}(t)$ (see below) is also included for two state points. Note that all three quantities show the same long-time limit, i.e. the viscosity does not depend on the way it is calculated. At intermediate times, the integral of $C_{\sigma\sigma}(t)$ and its fitting are in perfect agreement, but the integral of the fitted function is less noisy. Thus, we will calculate viscosities using the Einstein relation in Eq. 9.

The viscosity, as given by the long-time plateau, grows with increasing particle density, as shown in Fig. 3. This increase is consistent with a power-law, diverging at the transition point estimated from the structural relaxation time and from the diffusion coefficient, $\phi_c^G = 0.594$ [40]. The exponent for this power-law $\gamma_\eta = 2.74$ is similar to γ_τ but different from γ_D, as reported in Table I.
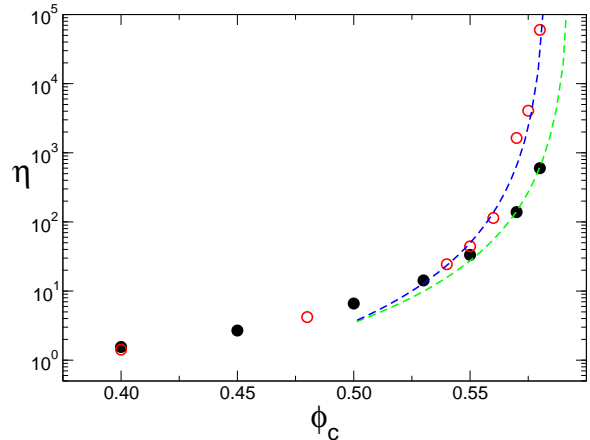

FIG. 3: Viscosity of soft (full black circles) and hard (empty red circles) spheres as a function of particle packing fraction, approaching the glass transition. Lines are power law fits to points with $\phi > 0.50$. The values of the critical packing fraction have been fixed to the previously determined values (see Table I), i.e. $\phi_c^G = 0.594$ and $\phi_c^G = 0.584$ for soft and hard sphere respectively. The corresponding fitting exponents γ_η are 2.74 and 2.9.

For hard spheres, path $1A$, we only show the integrated squared non-diagonal terms — obtained from Eq.11 — in Fig. 4. These results are obtained averaging over 20 independent starting configurations and over time for a minimum of $70\tau_\alpha$, where τ_α is the density relaxation time at the wavelength corresponding to the nearest-neighbour peak. The behaviour of the curves is very similar to that shown above for model B, and the viscosity, also shown in Fig. 3, increases as the glass transition is approached. A power-law divergence with exponent $\gamma_\eta \simeq 2.9$ is observed for the viscosity, with transition point at $\phi_c^G = 0.584$,

slightly lower than for V_{sc}. The value of the exponent is, again, in good agreement with γ_τ but quite different from γ_D.
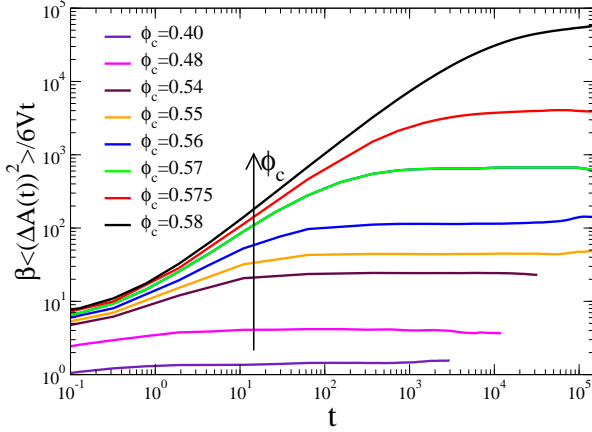

FIG. 4: $\beta < (\Delta A(t))^2 > /6Vt$ (with $\beta = 1$) for hard spheres, along path 1A.

B. Attractive glass: Path 2

In this section, we analyse the viscoelastic behaviour close to the attractive glass. As discussed above, for this purpose we use model B for which the liquid-gas separation is suppressed by the presence of the added repulsive barrier, allowing for the study of low density ($\phi_c = 0.40$) in a homogeneous system. In Fig. 5, we present again the stress correlation functions and the calculation of the viscosity by integrating the squared stress tensor non-diagonal terms. The attraction between particles induces a minimum after the short time (microscopic) relaxation, which introduces a negative correlation at intermediate attraction strengths. The origin of this minimum is similar to that in the velocity auto-correlation function, although here it is caused by stretching and rebound of the bonds. At high attraction strength, the correlation is positive again at all times, and after the minimum, $C_{\sigma\sigma}(t)$ shows the development of a two-step decay and a large increase of the value at zero time $C_{\sigma\sigma}(0)$, similarly to the phenomenology observed for the repulsive glass. This indicates that the system is becoming solid-like.

$\langle (\Delta A(t))^2 \rangle$, shown in the lower panel of Fig. 5, grows dramatically upon increasing the attraction strength. The long time limit value, η, is shown in Fig. 6 as a function of attraction strength. The data can be fitted using a power law divergence as a function of the distance from the transition, $\Gamma - \Gamma^G$, where Γ^G is reported in Table II. The exponent $\gamma_\eta = 3.16$ is again in good agreement with γ_τ.
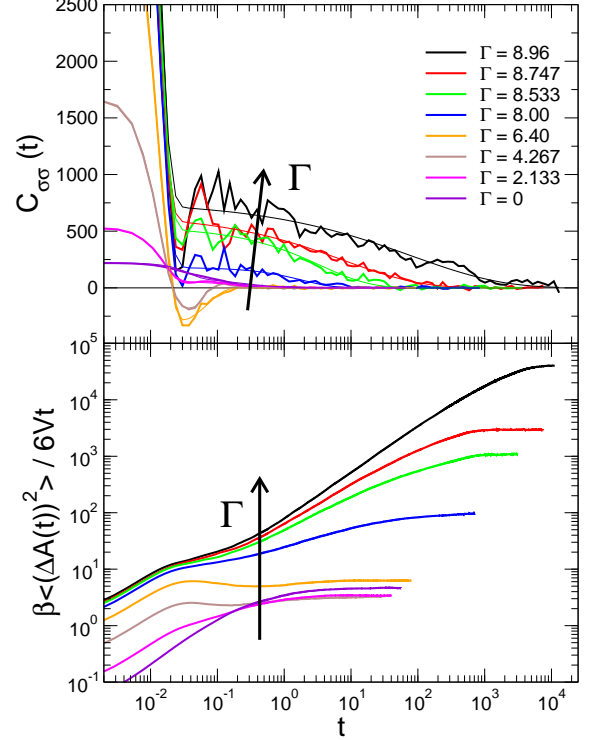

FIG. 5: Stress correlation function $C_{\sigma\sigma}(t)$ (upper panel) and $\beta < (\Delta A(t))^2 > /6Vt$ (lower panel) for different state points along the isochore $\phi_c = 0.40$. The thin lines in the upper panel represent empirical fittings to $C_{\sigma\sigma}(t)$, eq. (see section V for details).

C. Reentrance region: Path 3

As discussed above, path 3 is a high density isochoric path, where the attractive and repulsive glass lines are about to merge. Varying the attraction strength, the system can be studied in states close to the repulsive or to the attractive glass. This path is studied only with system A, because the short interaction range of the studied SW opens up a large fluid region between the two glasses.

Fig. 7 shows $\langle (\Delta A(t))^2 \rangle / t$ calculated using Eq.11. The corresponding viscosity is reported in Fig. 6 as a function of Γ. As expected in this region, the viscosity increases both at low temperature, due to the proximity of the attractive glass, and at high temperature, because of the nearby repulsive glass. A power law divergence describes the attractive glass increase of η with exponent $\gamma_\eta \simeq 3.75$, i.e. the same that is found also for the density relaxation time γ_τ. Data refer to an average over 20 independent starting configurations and over time for a minimum of $200\tau_\alpha$. A pronounced reentrant behaviour, covering two full decades toward both limits, is observed in η, similar to that reported previously for the diffusion coefficient D
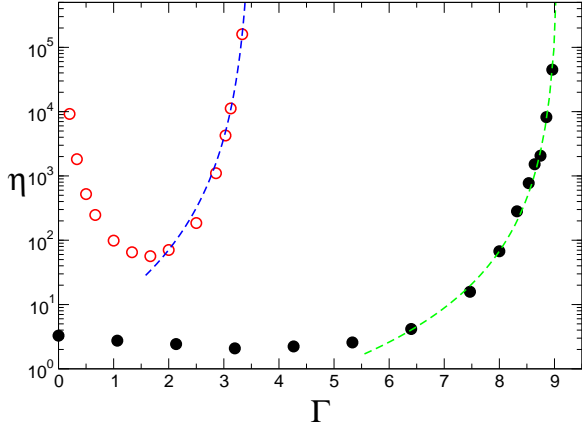
FIG. 6: Viscosity approaching the attractive glass transition along path 2 (full black circles), and in the reentrant region along path 3 (empty red circles), as a function of attraction strength. Lines represent power-law fittings (with values of the critical attraction strength fixed to the previously determined values reported in Table II), with exponents γ_η equal to 3.16 for path 2 and 3.75 for the attractive side of the reentrant path 3.
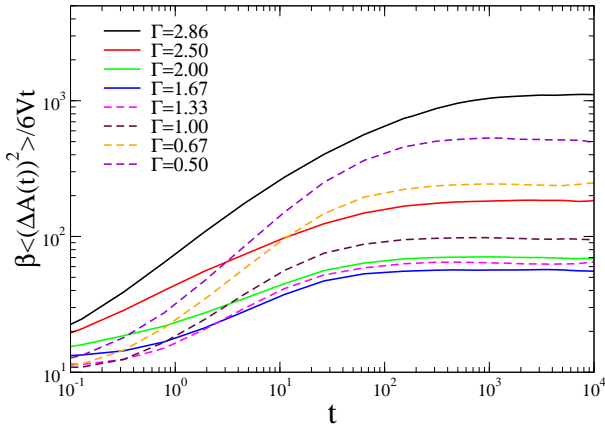
in the same system[23].

FIG. 7: $\beta < (\Delta A(t))^2 > /6Vt$ for different attraction strength Γ along the isochore $\phi_c = 0.58$ for path 3A. On decreasing Γ, the long time limit first decreases (full lines) and then increases again (dashed lines), resulting in a pronounced reentrant behaviour of the viscosity.

V. COMPARISON OF $C\sigma\sigma(t)$ WITH MODE COUPLING THEORY

MCT predicts[42] that the stress correlation function is related to an integral over all wavevectors of the density correlation functions:

$$C_{\sigma\sigma}(t) = \frac{k_B T}{60\pi^2} \int_0^\infty dq\, q^4 \left[\frac{d \ln S(q)}{dq} \Phi_q(t) \right]^2 \quad (12)$$

We theoretically calculate $C_{\sigma\sigma}(t)$ along two paths analogous to paths 1B and 2 studied in simulations, to compare the full time-behaviour of the stress correlation function. Hence, we study:
(i) a one-component hard sphere system with increasing ϕ, using the Percus-Yevick (PY) structure factor as input;
(ii) a one-component AO model with size ratio $q = 0.1$ at fixed packing fraction $\phi = 0.40$. Here $S(q)$ is calculated using PY closure for the two-component Asakura-Oosawa mixture. This model mixture is composed of HS colloidal particles and ideal-gas polymers with HS interactions between polymers and colloids[43]. The obtained colloid-colloid structure factor is used as input to a one-component MCT, a treatment based on the validity of an effective one-component description for small polymer-colloid size ratio[44, 45]. We did not use the fundamental measure density functional theory [46, 47] which yields analytical expressions for $S_{ij}(k)$ as done previously[48] because within this closure the system shows spinodal instability before MCT would actually give a glass. This is not the case with PY closure for which only a very tiny increase in the structure factor at small q is found approaching the MCT transition.

We solved the full dynamical MCT equations, as well as their long time limit, to calculate the viscoelastic properties close to the glass transition. We used a grid a 1500 wave-vectors with mesh $\Delta q = 0.314$.

The long-time limit of the integrand of Eq. 12,

$$I(q) = \lim_{t\to\infty} q^4 \left[\frac{d \ln S(q)}{dq} \Phi_q(t) \right]^2 = q^4 \left[\frac{d \ln S(q)}{dq} f_q^c \right]^2 \quad (13)$$

is plotted as a function of $q\sigma$, in Figure 8 for both studied systems, f_q^c being the critical non-ergodicity parameter at the MCT transition. The same figure reports also f_q^c and the input static structure factor, also at the transition, $S^c(q)$.

For the repulsive glass we find that the dominant contribution to the integral is provided by the wave-vector region around the nearest-neighbour peak, i.e. $q^*\sigma \approx 6.5$. For the attractive glass, on the other hand, the dominant contribution is found at much larger q-values, i.e. $q^*\sigma \approx 24$ (in the region of the fourth peak of $S(q)$) providing another confirmation of the importance of small length-scales in the localization properties of such a glass [41]. Moreover, in this case, the integrand is not just peaked around a specific value, but it is rather spread

within a very large q-interval. The amplitude of the integrand is also much larger in the case of the attractive glass as compared to the repulsive glass.
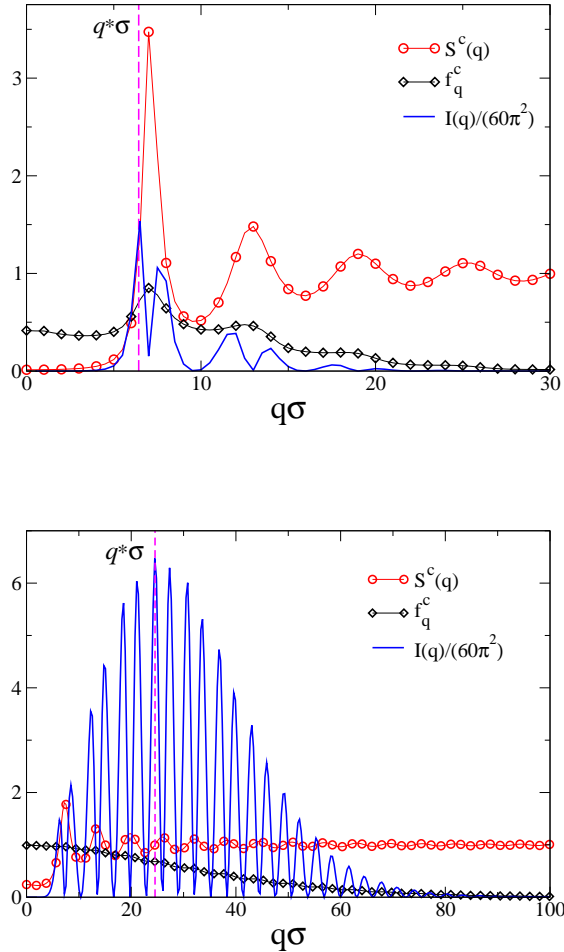
a small discrepancy at very long times. We attribute this difference to the fact that, in the case of attractive glasses, a large window of wavevectors contributes to the decay of the stress autocorrelation function (see Fig. 8).

FIG. 8: Mode coupling contributions to the viscosity $I(q)/(60\pi^2)$, with $I(q)$ defined in Eq. 13. The wavevector at which $I(q)$ is maximum, $q^*\sigma$, is ≈ 6.5 for the repulsive glass and ≈ 24 for the attractive glass. To compare, we report in the same figure also the $q-$dependence of the critical non-ergodicity parameter f_q^c and of the static structure factor $S^c(q)$.

We can then compare in the upper panel of Fig. 9 the theoretical stress correlation function with the squared theoretical density correlator $\phi_{q^*}^2(t)$ at the maximum of $I(q)$. We show two state points, one close to the repulsive glass and the other state close to the attractive one. Apart from an amplitude scaling factor, the dominant contribution is already sufficient to describe the long-time behaviour of $C_{\sigma\sigma}(t)$ for both attractive and repulsive glasses. However, for the attractive glass case, the decay of the squared density correlation shows a slightly smaller stretching as compared to $C_{\sigma\sigma}(t)$, which causes
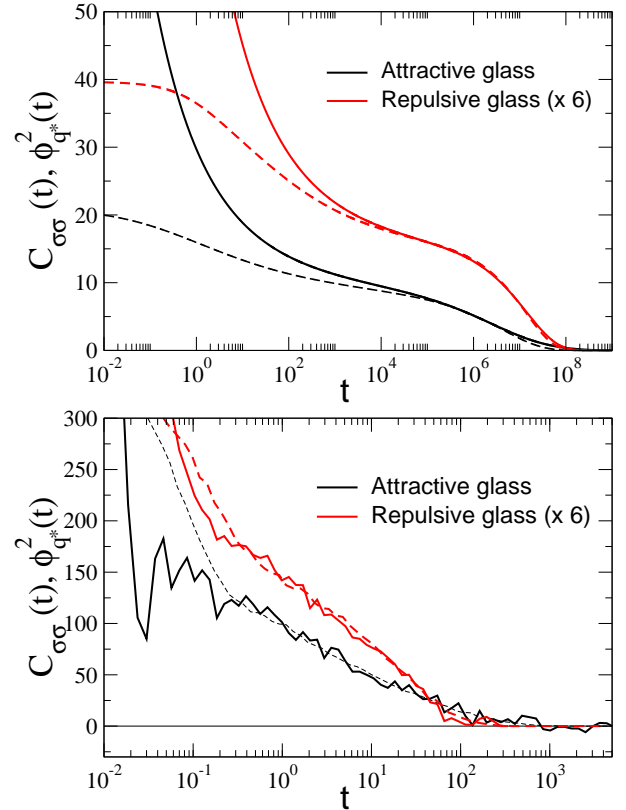

FIG. 9: Stress correlation function $C_{\sigma\sigma}(t)$ (full lines) for repulsive and attractive glasses calculated within MCT (top) and from simulations (bottom). Dashed lines are the squared density correlation functions $\phi_{q^*}^2(t)$, arbitrarily scaled in amplitude to overlap the long time behavior. For the MCT data, the wavevector q^* is the one reported in Fig. 8, while in the simulation panel it is the one which provides the best long-time overlap between $\phi_{q^*}^2(t)$ and $C_{\sigma\sigma}(t)$.

In the lower panel of Fig. 9, the time dependence of both $C_{\sigma\sigma}(t)$ and $\phi_{q^*}^2(t)$, as calculated from the simulation data, are also plotted. Here q^* is the wavevector at which the agreement between the time dependence of $C_{\sigma\sigma}(t)$ and $\phi_{q^*}^2(t)$ is optimal. The q^* values found in this way, respectively $q^*\sigma \approx 7.5$ and $q^*\sigma \approx 26$, agree very well with those predicted by the theory[40]. Moreover, the behaviour of $C_{\sigma\sigma}(t)$ is well-described (within the numerical error) by a single squared density correlator for both glasses. The small discrepancy which was observed in the MCT data for the attractive glass is probably buried within the numerical noise.

Finally we want to compare the elastic moduli for both glasses in the theoretical and numerical calculations. In order to calculate elastic and viscous moduli, the stress

ϕ_c	$C_{\sigma\sigma}(0)$	A	τ_0	τ_1	β
0.58	181	0.18	0.024	13.30	0.509
0.57	156	0.16	0.026	3.56	0.665
0.55	134	0.15	0.024	1.18	0.759
0.53	83	0.23	0.025	0.20	0.421
0.50	34	0.39	0.024	0.03	0.353

TABLE III: Parameters of the fitting of $C_{\sigma\sigma}(t)$ for states close to glass transition for soft-spheres (path 1B).

ϕ_p	$C_{\sigma\sigma}(0)$	A	τ_0	τ_1	β
0.42	1650	0.077	0.011	81.48	0.325
0.41	1506	0.072	0.011	8.09	0.389
0.40	1470	0.061	0.011	3.49	0.585
0.39	1404	0.071	0.012	1.90	0.949
0.30	724	-0.085	0.013	0.07	1.757

TABLE IV: Parameters of the fitting of $C_{\sigma\sigma}(t)$ for states close to attractive glass transition (Path 2).

	$C_{\sigma\sigma}(0)$	f_σ	$C_{\sigma\sigma}^{MCT}(0)$	f_σ^{MCT}
Path 1B	181	32	400	3
Path 2	1650	127	6000	100

TABLE V: Approximate values of initial value of the stress correlation value $C_{\sigma\sigma}(0)$ and height of the plateau, f_σ for paths 1B and 2. The first two columns refer to simulation data and the last two to theoretical MCT predictions.

correlation functions calculated from simulations have to be Fourier transformed: $G(\omega) = i\omega\tilde{C}(\omega)$, where $\tilde{C}(\omega)$ is the Fourier transform of $C_{\sigma\sigma}(t)$. However, due to the noise in the correlation function, direct transformation produces very low quality results. Thus, we have fitted $C_{\sigma\sigma}(t)$ with empirical functional forms close to both glasses before performing the Fourier transform. We have chosen

$$
\begin{aligned}
C_{\sigma\sigma}(t) = {} & C_{\sigma\sigma}(0)\,\{f(t/\tau_0) + \\
& A(1 - f(t/\tau_0))\exp\{-(t/\tau_1)^\beta\}\}
\end{aligned} \quad (14)
$$

where $f(x)$ is an even function that describes the short time relaxation of $C_{\sigma\sigma}(t)$: $f(x) = 1/(1 + x^2)$ for the repulsive glass (Fig. 2) and $f(x) = \exp\{-x^2\}$ for the attractive glass (Fig. 5). τ_0 represents a microscopic time scale, which should be state-independent, whereas τ_1 gives the time scale for the stress final relaxation. The parameter A gives the amplitude of the stored stress (so that $A C_{\sigma\sigma}(0)$ is the height of the plateau in $C_{\sigma\sigma}(t)$) and β is the stretching exponent, which according to the MCT prediction should be roughly equal to the stretching exponent of the density-density correlation function at q^*.

In Table III we present the parameters of the fittings for $C_{\sigma\sigma}(t)$ for states along path $1B$, drawn in Fig. 2 as thin lines. As expected, τ_0 is state-independent and τ_1 increases substantially when the glass transition is approached. A and β are correctly estimated only when the second relaxation is noticeable, i.e. above $\phi_c = 0.55$; in these cases the amplitude is almost constant and β is compatible with the value obtained from the density correlation function at q^*, $\beta = 0.52$ [38].

The parameters of the fittings for the attractive glass (path 2), shown in Fig. 5, are given in Table IV. As before, τ_0 is almost constant, whereas τ_1 increases dramatically upon increasing the attraction strength.

From the values of the fits, we can directly compare other quantities between theory and simulations: namely, the $t = 0$ value of the stress correlation function $C_{\sigma\sigma}(0)$ and the height of the long-time plateau f_σ for both glasses. The results from MCT and simulations are reported in Table V for both studied paths. For both glasses, the simulations provide a lower value of $C_{\sigma\sigma}(0)$ and a larger value of f_σ with respect to MCT. Although numbers are not important *per se* when comparing to MCT, the ratio $f_\sigma/C_{\sigma\sigma}(0)$ is wrong by one

order of magnitude for both attractive and repulsive glasses. This result seems to suggest that the factorization approximation[42] adopted to derive Eq.12 may be too severe, although the structural relaxation is apparently well described, as shown by the comparisons of Fig. 9.

We finally directly compare the elastic and viscous moduli $G'(\omega)$ and $G''(\omega)$ in Fig. 10 for repulsive (top)
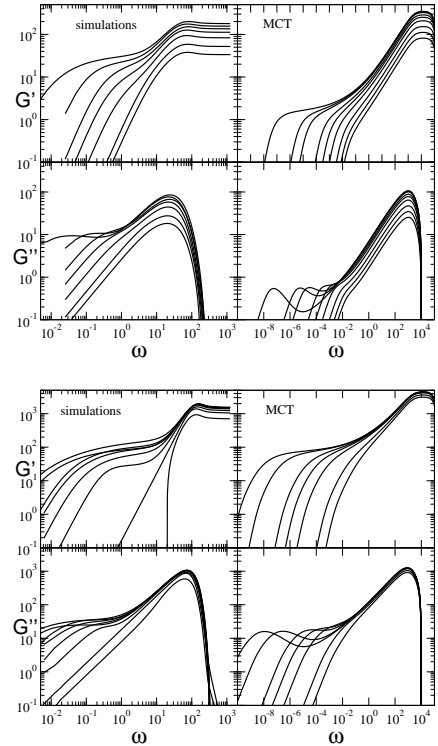

FIG. 10: Shear moduli G' and G'' from simulations (left) and MCT (right) for repulsive (top) and attractive glass (bottom).

and attractive glass (bottom). We observe qualitatively the same trends for both transitions in theory and simulations, despite a shift in the absolute numbers:

(i) an increase of $G'(\omega)$ at large-ω (but smaller than the microscopic frequency) with the approach to the glass transition;

(ii) the appearance of a minimum in G'' which moves to lower and lower ω with decreasing distance from the transition, in agreement with previous experimental and theroetical studies on both repulsive [49, 50] and attractive glasses [51, 52]. The minimum appears when $\epsilon \lesssim 0.01$ according to the theory ($\epsilon = |X_g - X|/X_g$, with X being either ϕ or Γ), and at slightly larger values of ϵ according to the simulations;

(iii) much larger moduli (up to one order of magnitude) for the attractive than for the repulsive glass. This observation holds both for theory and simulations and agrees well with recent rheological measurements for thermo-reversible sticky spheres[19, 53].

Overall, MCT correctly predicts the behavior of the viscoelastic properties on approaching both glass transitions. However, the results disagree again quantitatively, and more importantly in the ratio of the height of the plateau in G' (or minimum in G'') with respect to G'_∞ (or G''_{max}).

VI. BREAKDOWN OF STOKES-EINSTEIN RELATION

Finally, we discuss the breakdown of the Stokes-Einstein (SE) relation[54, 55, 56, 57, 58, 59, 60] close to the glass transition for all different studied paths.

We start by examining path I. Fig. 11 shows the SE relation for the hard sphere binary system and the soft sphere polydisperse system. To allow for a unifying picture, we plot the results as a function of the relative distance to the estimated glass transition ($\phi_g - \phi$). At low and moderate density, far from the transition the data are consistent with SE, although different values limits are obtained for model A or B; whereas the former takes the stick value, $D\eta/T = (3\pi\sigma)^{-1}$, the latter goes to the slip limit: $D\eta/T = (2\pi\sigma)^{-1}$. The reason for this difference is not clear [61, 62, 63]. In both cases, as the system approached the glass transition, the SE relation breaks down significantly, both in the form $D\eta$ and $D\tau$ (see inset).

Fig. 12 shows the SE relation for the attractive glass case (path II) and along the reentrance (path III). The former case is rather clean, and allows us to access a breakdown by two orders of magnitude with respect to the typical SE value, both in $D\eta/T$ and $D\tau$ (inset). For both paths, at large Γ (low T) a clear breakdown of both $D\tau$ and $D\eta/T$ is observed for the attractive glass.

For path III (reentrance case), one has to bear in mind that the path becomes parallel to the repulsive glass line at small Γ (see Fig. 1) and the increase is limited to the one observed in the HS case at the same packing. For
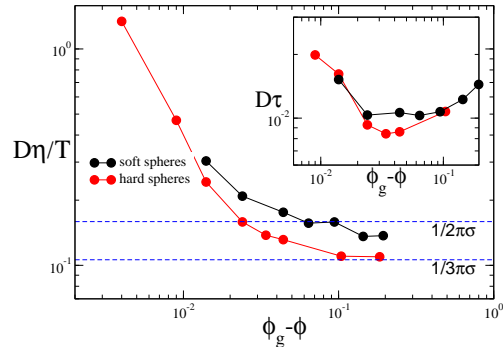

FIG. 11: Breakdown of the SE relation for $D\eta/T$ approaching the repulsive glass transition for paths 1A (empty red circles) and 1B (full black circles). For the hard sphere case, $T = 1$. Lines are guide to the eye. The two horizontal dashed lines mark the slip and stick values of the SE relation. Inset: $D\tau$ for the same paths.

this path we have also performed BD simulations. The BD results, also shown in Fig. 12 coincide with the MD data at all state points investigated, confirming that the SE behavior close to both repulsive and attractive glass transitions does not depend on the microscopic dynamics.

Data in Fig. 11 and Fig. 12 provide evidence that the breakdown of the SE is a phenomenon which can be observed in the vicinity of both the repulsive and the attractive glass transitions. Within the investigated state window, it appears that the magnitude of the breakdown is enhanced in the attractive glass case, speaking for the presence of more intense dynamical heterogeneities [64, 65, 66] when confinement is originated by short-range bonds rather than by the excluded volume caging.

VII. CONCLUSIONS

In this article we reported the behavior of the viscosity in two models for short-range attractive colloids along three different paths in the attraction-strength packing-fraction plane. Along the first path, the system approaches the repulsive hard-sphere glass transition. Along the second path, it approaches the attractive glass. The third path is chosen in such a way that the system moves continuously from the repulsive to the attractive glass at constant packing fraction in the so-called re-entrant region[67]. In this case, we have also compared brownian and newtonian simulation results, confirming that the viscosity is independent on the microscopic dynamics, in agreement with results based on the decay of density fluctuations in atomic liquids[68].

We find that the increase of the viscosity on approaching the glass transition is consistent with a power-law divergence. The divergence of η can be described with the same exponent and critical packing fraction previ-
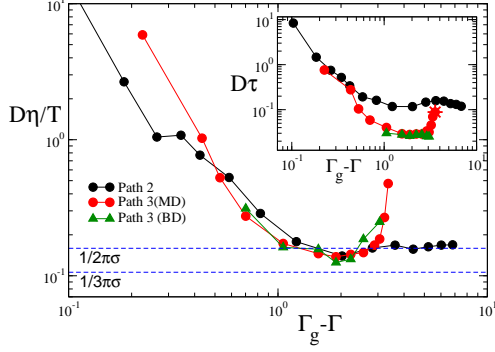
FIG. 12: Breakdown of the SE relation for $D\eta/T$ approaching the attractive glass transition for paths 2 (circles) and 3 (squares-MD and triangles-BD). Note the partial breakdown also at high T for the reentrant path due to the closeby repulsive glass. The two horizontal lines mark the slip and stick SE values. Inset: $D\tau$ for the same paths. The star indicates the HS value for path 3.

ously found for the collective relaxation time, but with an exponent different from the one that characterizes the divergence of the diffusion coefficient. This holds for both attractive and repulsive glass.

As previously observed for diffusion and collective relaxation, the viscosity shows a non monotonic behavior with the attraction strength in the reentrant region (path III), confirming once more the validity of the theoretical MCT predictions.

To provide a connection between density relaxation and visco-elastic behavior we investigate the leading density fluctuation contributions to the decay of the stress autocorrelation function within MCT. Interestingly, for the case of the repulsive glass, it is possible to identify a small range of wave-vectors (not far from the first peak of the structure factor) which are responsible for the visco-elastic behavior. In the case of the attractive glass, instead, the decay of the stress is associated to a much larger window of wavevectors, centered at much larger values. In this respect, the visco-elastic analysis con-

firms that dynamic arrest is driven by the short-lengh scale introduced by the bonding. We also compare the simulation results for the frequency dependence of the elastic moduli with corresponding theoretical MCT predictions, finding a substantial qualitative agreement.

Finally, we have evaluated the Stokes-Einstein relation. A clear breakdown of the relation is observed on approaching both glass lines, consistent with the different exponents characterizing the power-law dependence of diffusion and viscosity. The breakdown is particularly striking on approaching the attractive glass (a variation of the product $D\eta/T$ of up to two order of magnitude in the investigated range). Recent theoretical work on MCT seems to provide insights that could be useful to reconcile the decoupling of self-diffusion and viscosity (or relaxation time) within MCT[57]. It would be interesting in the future to deepen our knowledge of the connection between SE breakdown and the presence of dynamic heterogeneities, which has been previously studied for the same model[64].

Note: While finalizing the manuscript, we become aware of a numerical study by Krekelberg *et al.* (cond-mat/07050381) which also reports the non-monotonic behavior of the viscosity along the reentrant path and the breakdown of the SE relation. In that work, Krekelberg *et al.* seek a connection between the structural and dynamical properties of the system. We show here that MCT predicts correctly the properties of the system upon approaching the glass transitions, i.e. the connection between structure and dynamics is the non-trivial one provided by MCT.

VIII.   ACKNOWLEDGMENTS

[1] R. Mezzenga, P. Schurtenberger, A. Burbidge, and M. Michel, Nature Materials pp. 729–740 (2005).
[2] R. P. Sear, Curr. Opin. Coll. Interf. Sci. **11**, 35 (2006).
[3] V. Trappe and P. Sandkühler, Curr. Op. Coll. Interf. Sci. **8**, 494 (2004).
[4] L. Cipelletti and L. Ramos, J. Phys.:Condens. Matter **17**, 253 (2005).
[5] F. Sciortino and P. Tartaglia, Adv. Phys. **54**, 471 (2005).
[6] E. Zaccarelli, J. Phys.:Condens. Matter (2007), in press.
[7] A. Yethiraj and A. V. Blaaderen, Nature **421**, 513 (2003).
[8] V. Prasad, D. Semwogerere, and E. R. Weeks, J. Phys.: Condens. Matter **19**, 3102 (2007).
[9] L. Fabbian, W. Götze, F. Sciortino, P. Tartaglia, and F. Thiery, Phys. Rev. E **59**, 1347 (1999).
[10] J. Bergenholtz and M. Fuchs, J. Phys.: Condens. Matter **11**, 10171 (1999).
[11] K. A. Dawson, G. Foffi, M. Fuchs, W. Götze, F. Sciortino, M. Sperl, P. Tartaglia, T. Voigtmann, and E. Zaccarelli, Phys. Rev. E **63**, 011401 (2001).
[12] W. Götze and M. Sperl, Phys. Rev. E **66**, 011405 (2002).
[13] M. Sperl, Phys. Rev. E **68**, 031405 (2003).
[14] K. N. Pham, A. M. Puertas, J. Bergenholtz, S. U. Egelhaaf, A. Moussaïd, P. N. Pusey, A. B. Schofield, M. E. Cates, M. Fuchs, and W. C. K. Poon, Science **296**, 104

(2002).

[15] T. Eckert and E. Bartsch, Phys. Rev. Lett. **89**, 125701 (2002).

[16] S. H. Chen, W.-R.Chen, and F. Mallamace, Science **300**, 619 (2003).

[17] K. N. Pham, S. U. Egelhaaf, P. N. Pusey, and W. C. K. Poon, Phys. Rev. E **69**, 1 (2004).

[18] J. Grandjean and A. Mourchid, Europhysics Letters **65**, 712 (2004).

[19] T. Narayanan, M. Sztucki, G. Belina, and F. Pignon, Phys. Rev. Lett. **96**, 258301 (2006).

[20] W. Götze, *Liquids, Freezing and the Glass Transition* (North-Holland Amsterdam, 1991), pp. 287–503.

[21] A. M. Puertas, M. Fuchs, and M. E. Cates, Phys. Rev. Lett. **88**, 098301 (2002).

[22] G. Foffi, K. A. Dawson, S. V. Buldrey, F. Sciortino, E. Zaccarelli, and P. Tartaglia, Phys. Rev. E **65**, 050802 (2002).

[23] E. Zaccarelli, G. Foffi, K. A. Dawson, S. V. Buldrey, F. Sciortino, and P. Tartaglia, Phys. Rev. E **66**, 041402 (2002).

[24] A. Puertas, M. Fuchs, and M. E. Cates, Phys. Rev. E **67**, 031406 (2003).

[25] Z. Cheng, J. Zhu, P. Chaikin, S.-E. Phan, and W. Russel, Phys. Rev. E **65**, 041405 (2002).

[26] M. Fuchs and M. E. Cates, Faraday Discussion **123**, 267 (2003).

[27] S. Shah, Y.-L. Chen, K. Schweizer, and C. Zukoski, J. Chem. Phys. **119**, 8747 (2003).

[28] E. Zaccarelli, F. Sciortino, S. V. Buldyrev, and P. Tartaglia, *Short-ranged attractive colloids: What is the gel state?* (Elsevier, Amsterdam, 2004), pp. 181–194.

[29] M. G. Noro and D. Frenkel, J. Chem.Phys **113**, 2941 (2000).

[30] M. A. Miller and D. Frenkel, J. Chem.Phys **121**, 535 (2004).

[31] F. Sciortino, P. Tartaglia, and E. Zaccarelli, Phys. Rev. Lett. **91**, 1 (2003).

[32] D. C. Rapaport, *The Art of Molecular Dynamic Simulation* (1995).

[33] G. Foffi, C. D. De Michele, F. Sciortino, and P. Tartaglia, Phys. Rev. Lett. **94**, 078301 (2005).

[34] A. Scala, T. Voigtmann, and C. De Michele, J. Chem. Phys. **126**, 134109 (2007).

[35] A. M. Puertas, M. Fuchs, and M. E. Cates, Phys. Rev. E **67**, 031406 (2003).

[36] B. Alder, D. Gass, and T. Wainwright, J. Chem. Phys. **53**, 3813 (1970).

[37] J. R. Melrose, EuroPhys. Lett. **19**, 51 (1992).

[38] T. Voigtmann, A. M. Puertas, and M. Fuchs, Phys. Rev. E **70**, 061506 (2004).

[39] A. M. Puertas, M. Fuchs, and M. E. Cates, J. Phys. Chem. B **109**, 6666 (2005).

[40] A. M. Puertas, E. Zaccarelli, and F. Sciortino, J. Phys.:Condens. Matter **17**, L271 (2005).

[41] O. Henrich, A. Puertas, M. Sperl, J. Baschnagel, and M. Fuchs, cond-mat/07050637 (2007).

[42] G. Nägele and J. Bergenholtz, J. Chem. Phys. **108**, 9893 (1998).

[43] S. Asakura and F. Oosawa, J. Polym. Science **33**, 183 (1958).

[44] M. Dijkstra, J. M. Brader, and R. Evans, J. Phys.: Condens. Matter **11**, 10079 (1999).

[45] M. Dijkstra, R. van Roij, and R. Evans, J. Chem. Phys. **113**, 4799 (2000).

[46] M. Schmidt, H. Löwen, J. M. Brader, and R. Evans, Phys.Rev.Lett. **85**, 1934 (2000).

[47] M. Schmidt, H. Löwen, J. M. Brader, and R. Evans, J. Phys.:Cond. Matt **14**, 9353 (2002).

[48] E. Zaccarelli, H. Löwen, P. P. F. Wessels, , F. Sciortino, P. Tartaglia, and C. N. Likos, Phys. Rev. Lett. **92**, 1 (2004).

[49] T. G. Mason and D. A. Weitz, Phys.Rev.Lett. **75**, 2770 (1995).

[50] M. Fuchs and M. R. Mayr, Phys.Rev E **60**, 5742 (1999).

[51] K. A. Dawson, G. Foffi, F. Sciortino, P. Tartaglia, and E. Zaccarelli, J. Phys.: Condens. Matter **13**, 9113 (2001).

[52] F. Mallamace, P. Tartaglia, W. R. Chen, A. Faraone, and S. Hsin Chen, J. Phys.:Cond. Matt **16**, 4975 (2004).

[53] M. Sztucki, T. Narayanan, G. Belina, A. Moussaïd, F. Pignon, and H. Hoekstra, Phys. Rev. E **74**, 051504 (2006).

[54] F. H. Stillinger and J. A. Hodgdon, Phys. Rev. E **50**, 2064 (1994).

[55] M. D. Ediger, Ann. Rev. Phys. Chem **51**, 99 (2000).

[56] S. K. Kumar, G. Szamel, and J. F. Douglas, J. Chem. Phys. **124**, 4501 (2006).

[57] G. Biroli and J.-P. Bouchaud, Journal of Physics Condensed Matter **19**, 5101 (2007).

[58] Y. Jung, J. P. Garrahan, and D. Chandler, Phys. Rev. E **69**, 061205 (2004).

[59] Y. Brumer and D. R. Reichman, Phys. Rev. E **69**, 041202 (2004).

[60] S. R. Becker, P. H. Poole, and F. W. Starr, Physical Review Letters **97**, 055901 (2006).

[61] P. Segré, S. Meeker, P. Pusey, and W. Poon, Phys. Rev. Lett. **75**, 958 (1995).

[62] C. D. Michele and D. Leporini, Phys. Rev. E **63**, 036701 (2001).

[63] A. Moreno, S. Buldyrev, E. L. Nave, I. Saika-Voivod, F. Sciortino, P. Tartaglia, and E. Zaccarelli, Phys. Rev. Lett. **95**, 157802 (2005).

[64] A. Puertas, M. Fuchs, and M. E. Cates, J. Phys. Chem. **121**, 2813 (2004).

[65] C. J. Dibble, M. Kogan, and M. J. Solomon, Phys. Rev. E **74**, 041403 (2006).

[66] Y. Gao and Kilfoil, Phys. Rev. Lett. (in press) (2007).

[67] F. Sciortino, Nature Materials **1**, 145 (2002).

[68] T. Gleim, W. Kob, and K. Binder, Phys. Rev. Lett. **81**, 4404 (1998).